Check for updates

On donor–acceptor-bridging intramolecular hydrogen bonds in NIR-TADF molecules†

Fabian Weber [ID] and Hirotoshi Mori [ID] *

Following a report that highlights the importance of intramolecular hydrogen bonds for improved NIR-TADF efficiency in CAT-1 [Leng *et al.*, *J. Phys Chem. A*, 2021, **125**, 2905], an intramolecularly doubly hydrogen-bonded base design is investigated and compared to singly and non-bonded derivatives. It is found that the potential to form more intramolecular hydrogen bonds correlates with decreasing internal reorganization energies in most of the designed structures. In addition, our proposed base design facilitates the desired interlocking of charge transfer donor-, linker- and acceptor-planes through steric gauche-interactions to both linker-plane sides, allowing to trap also smaller heterocyclic linkers.

Introduction

Nearly one decade has passed since the realization of the first application oriented, metal-free thermally-activated delayed fluorescence (TADF) molecules[1] and ever since, design concepts have been successfully applied to conquer more and more regions of the electromagnetic spectrum. This way, TADF molecules like CAT-1[2] (4-(4-(diphenylamino)phenyl)acenaphtho[1,2-*b*]pyrazine-3,8,9-tricarbonitrile) and CZ-MPS[3] (2,7-bis(3,6-di-*tert*-butyl-9*H*-carbazol-9-yl)-9,9-dimethyl-9*H*-thioxanthene 10,10-dioxide) with emitter wavelengths as low-energetic as 950 nm and as high-energetic as 389 nm have been reported, reaching from the near-infrared (NIR) all the way into the ultraviolet (UV) region. One recurring challenge in the development of TADF designs is to ensure a high rigidity of the structure across excited states to minimize the activation energy associated with the overall reverse intersystem crossing (rISC) process. Following the semi-classical expression of Marcus' theory, the rISC rate can be expressed as[4]

$$k = \frac{2\pi}{\hbar} \frac{|H_{\mathrm{SOC}}|^2}{\sqrt{4\pi\lambda k_{\mathrm{B}}T}} \exp\left(-\frac{(\Delta E_{\mathrm{ST}} - \lambda)^2}{4k_{\mathrm{B}}T\lambda}\right).$$

Besides the spin–orbit coupling term H_{SOC}, there are two major expressions that are direct molecular properties that can be optimized for. The first, ΔE_{ST}, represents the vertical energetic singlet–triplet gap at the reactant excited triplet state geometry. The second, λ, is the sum of internal and external reorganization energy after the transition from the triplet to the singlet state. Here, the external term λ_{ext} captures energetic changes in the surrounding (*i.e.* solvent relaxation), while the internal portion λ_{int} is limited to the reactant's structural relaxation. The latter is defined as the energy difference between the relaxed final state (*i.e.* the excited singlet at its relaxed structure) and the respective target energy, as seen from the reactant structure (*i.e.* the excited singlet energy at the relaxed triplet structure). Note for increasing the rISC rate in this expression, the typical focus lies with optimizing the exponential to become as close to 1 as possible by achieving small ΔE_{ST} and λ.

Comparing two Jablonski diagrams with high and low internal reorganization energies (see Fig. 1), one can find that there is an indirect connection between ΔE_{ST} and λ_{int}, such that lower λ_{int} may also result in lower ΔE_{ST} at the reactant geometry.

Especially in the low energetic regime where electronic excitation energies start to match those of vibrational excitation energies, low internal reorganization energies λ_{int} between the electronically excited state structures become decisive for the performance of TADF candidates.[5] One possible strategy, how this can be achieved in the CAT-1 structure (see left side of

Chuo University, Department of Applied Chemistry, Kasuga 1-13-27, 112-8551, Tokyo-to, Bunkyo-ku, Japan. E-mail: fweber13790@gmail.com; qc-forest.19d@g.chuo-u.ac.jp
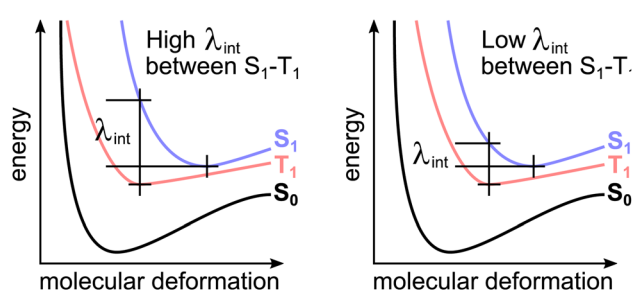
Fig. 1 Jablonski diagrams of a molecular system with high (left) and low (right) reorganization energy with ground state S_0 (black), excited singlet state S_1 (blue) and excited triplet state T_1 (red).
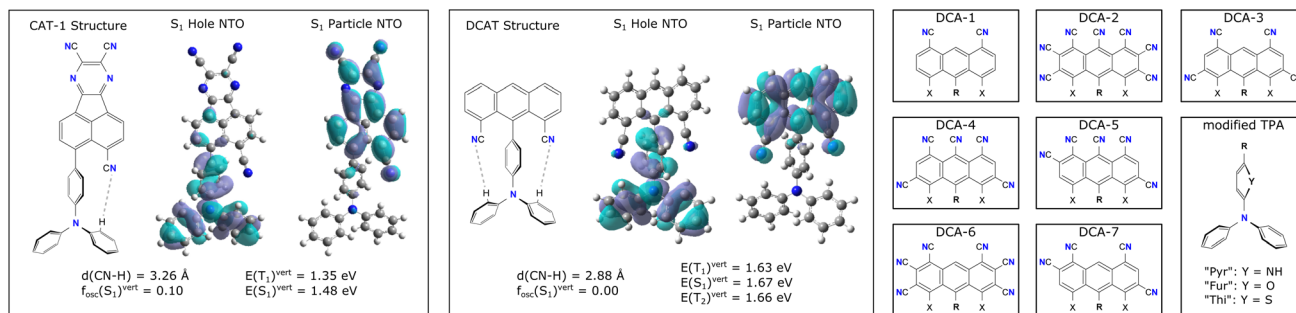
Fig. 2 Excited state properties and Lewis structures of CAT-1 (left) and unfunctionalized DCAT (middle). Dashed grey lines highlight potential hydrogen bonds. On the right, other building blocks considered for DCA acceptor and TPA-like donor units are shown. Note that the groups X on the acceptors may be either hydrogen or cyano groups, giving rise to the respective singly or zero hydrogen-bonded versions [1]DCA and [0]DCA.

Fig. 2) has recently been reported to lie in the use of intra-molecular hydrogen bonds to fixate the relative positions and rotations of charge-transfer (CT) donor and acceptor units.[6] In comparing CAT-1 with its non hydrogen-bonded counterpart TPAAP,[7] (3-(4-(diphenylamino)phenyl)acenaphtho[1,2-b] pyrazine-8,9-dicarbonitrile) Leng *et al.* found a lowered λ_{int} that may be responsible for its more efficient NIR-TADF process compared to TPAAP.

To build on top of this design principle, in this work we apply theoretical calculations to investigate the properties of potentially doubly hydrogen-bonded 4,5-dicyanoanthracene-10-triphenylamine (DCAT) derivatives. In a first step, we use (time-dependent) density-functional theory (TD-DFT) to optimize the structures at their electronic ground and selected excited states. Using these structures we then evaluate reorganization energies λ_{int}, spin–orbit coupling matrix elements (SOCME) between states that are relevant for TADF and correlations with the hydrogen bond properties. Computational details are provided in the ESI.†

Results and discussion

Fig. 2 shows the Lewis representations of CAT-1 and the base DCAT structure with their respective hole and particle natural transition orbitals (NTO)[8] that describe the first excited singlet state in TD-DFT quality at the ground state geometry. At these geometries, CAT-1 and DCAT exhibit vertical excitation energies of $E(S_1) = 1.35$ eV and 1.67 eV, respectively. As can be seen from NTO analysis, the S_1 state of both molecules describes a charge transfer (CT) in which the triphenylamine (TPA) unit acts as the charge donor[9] and the respective other half of the molecule acts as the acceptor. For CAT-1, a vertical singlet–triplet gap ΔE_{ST} of 0.13 eV is found, whereas DCAT shows a gap of 0.01 eV. While small ΔE_{ST} in principle promote the rate of rISC, it is also known that too low gap energies indicate a strong spatial separation of the frontier molecular orbitals involved in the excitation,[10] thus leading to dark singlet states with transition dipole moments of zero. Finally, both molecules feature groups of atoms that may form hydrogen bonds (CN–HC) between the acceptor unit and TPA at distances of 3.26 Å and 2.88 Å for CAT-1 and DCAT respectively. Note, that natural bond orbital (NBO) analysis[11] (*cf.* Fig S1 in the ESI†) confirms that there were indeed electrostatic

binding interactions in all investigated structures in the range of 0.4 up to 3.6 kcal mol^{-1} per site, suggesting that these are weakly to moderately hydrogen bonding groups. For the sake of simplicity, in the following these shall be, however, just referred to as hydrogen bonds.

Starting from the base DCAT architecture, three types of modifications were made in order to find candidate structures that achieve both non-zero transition dipole moment singlet states, as well as red-shift the excitation energies further into the NIR regime (*i.e.* below 1.65 eV, or longer than 750 nm[12]). Firstly, the 4,5-dicyanoanthracene (DCA) unit was decorated with further cyano-groups, since a higher CT acceptor strength was expected to reduce the excitation energy.[5] Such modifications will be expressed by a number code, like DCA-1 and DCA-2 (see right panels of Fig. 2). Secondly, the phenyl ring that connects the nitrogen of the TPA unit with the anthracene was substituted for small heterocycles such as pyrrole, furanyl and thiophenyl. These modified donors will be referred to as TPA-like and the ring in question is referred to as the (π-)linker. Their substitutions will be expressed by name extensions "Pyr", "Fur" and "Thi" (*e.g.* DCAT-1-Pyr). Finally, some DCA-like acceptors with only one or zero cyano-groups pointing towards the donor were modeled to investigate the effects of a step wise introduction of hydrogen bonds. Such structures carry a superscript prefix [1] or [0] to denote a smaller number of possible bonds (*e.g.* [1]DCAT). Note that by this logic, the zero-bonded variant of CAT-1 is the TPAAP molecule.[7]

With this three-fold functionalization strategy we arrive at a small family of molecules in which several were identified as potential candidates for NIR-TADF in theoretical calculations. Fig. 3 shows an overview of the excited singlet and triplet excitation energies of all investigated derivatives, color coded by the respective linker used. Note that higher opacity of the circles further serves as a rough scale of relatively higher S_1 transition dipole moments. While all markers show the respective molecule's S_1 state, the triplet state energy was chosen to be the closest lying to the S_1 state (that is T_n, *i.e.* either T_1 or T_2). This choice was made as in many instances more than one triplet state was in energetic vicinity to the S_1 state and supported a useful excited state character based on its spin-free NTOs and spin–orbit coupling matrix elements (SOCME). Also, previous studies have shown that the T_1 state does not have to be the
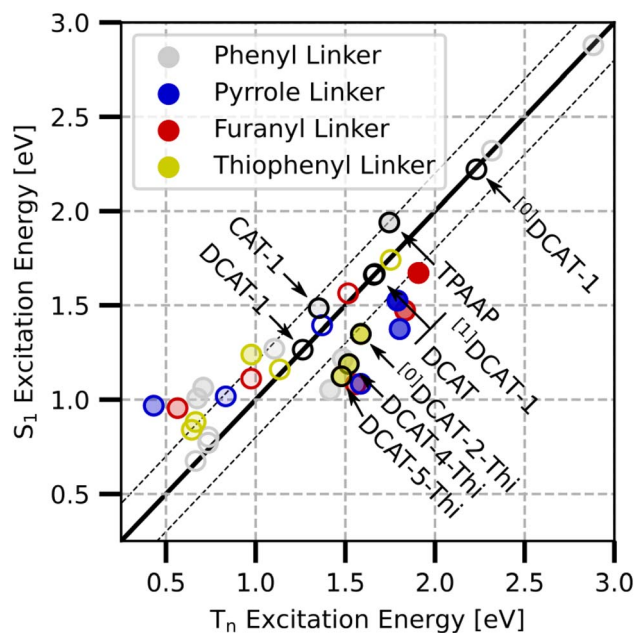
Fig. 3 Overview of excited state energies. Note that the triplet state energy was taken from the triplet state with the smallest relative singlet–triplet gap to the S_1 state. The diagonal (dashed) line marks the case of $E(S_1) = E(T_n)$ (± 0.2) and circles are color coded with respect to their linker. Higher opacity indicate molecules with higher transition dipole moments for S_1.

Fig. 4 Excitation properties grouped with dashed lines by acceptor unit (a) using different TPA(-like) donors at position R; and zero, one or two cyano groups at positions X. (b) Excited state energies of S_1 (blue) and closest lying T_n (red) and their resulting singlet–triplet-gap (c) at the excited state geometries of T_1 (clean bars, diamonds) and S_1 (hatched bars, circles). (d) Spin–orbit coupling matrix elements of the S_1/T_1 (left bar) and S_1/T_2 (right bar) transitions with respect to excited state optimized structures (clean and hatched).

TADF-active state, and that higher excitations may also serve as the major TADF-active triplet state.[13]

Considering all DCAT derived molecules contained in this study, at the ground state geometry we find vertical S_1 transition dipole moments up to 0.59 and singlet excitation energies in the range of 0.68 to 2.88 eV. Table 1 shows the detailed properties of a few selected molecules at the ground state and T_1 optimized structures that serve as a reference or may be interesting for NIR-TADF application. A full version of the studied molecules' structures and their related data can be found in detail in Table S1 and at the end of the ESI.†

Following Kasha's rule,[14] the lowest excited singlet state S_1 is presumably responsible for the main portion of fluorescence in TADF. Likewise, for the manifold of triplet states, the one that is expectedly the most populated over time is the lowest excited triplet state T_1 – which, as mentioned earlier, is however not necessarily also the one that is best suited for rISC. Hence, to get a more in-depth view which molecules of the DCAT family may
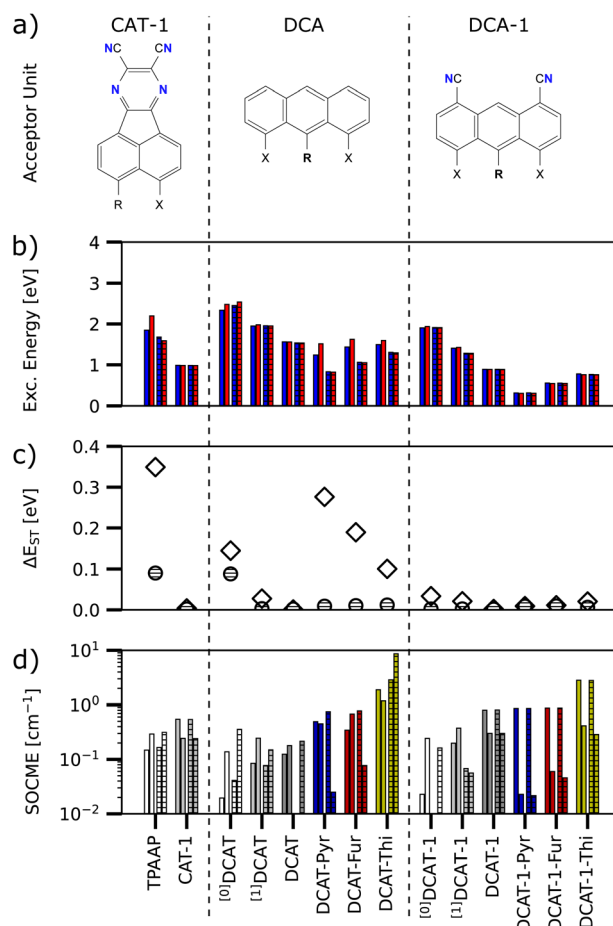
be suitable for NIR-TADF, all structures were optimized and re-evaluated at the respective lowest lying excited singlet and triplet states. Fig. 4 shows a comparative excerpt of the relevant data for selected excited state structures.

From the excitation energies (Fig. 4b), two trends within each subgroup of acceptor unit can be identified. Firstly, the

Table 1 Excitation properties of selected molecules. Values in parentheses were taken from the T_1 optimized structure, which we considered to be the most likely starting point of the overall TADF process[a]

Structure	E_{T_1} [eV]	E_{T_2} [eV]	E_{S_1} [eV]	ΔE_{ST} [eV]	$f_{osc}(S_1)$	λ_{int} [kcal mol^{-1}]	SOCME(S_1/T_1)	SOCME(S_1/T_2) [cm^{-1}]
CAT-1	1.35 (**0.98**)	2.06 (1.88)	1.48 (**0.99**)	0.13 (0.01)	0.20 (0.00)	0.026	(0.543)	(0.242)
DCAT	1.63 (0.91)	1.66 (**1.56**)	1.67 (**1.56**)	0.01 (0.00)	0.00 (0.01)	6.179	(0.124)	(0.180)
DCAT-1	1.26 (**0.89**)	1.49 (1.21)	1.27 (**0.89**)	0.01 (0.00)	0.00 (0.00)	0.005	(0.803)	(0.300)
[0]DCAT-2-Thi	0.86 (**0.36**)	1.59 (1.11)	1.35 (**0.37**)	0.24 (0.01)	0.38 (0.00)	0.004	(3.039)	(0.426)
DCAT-4-Thi	0.64 (**0.06**)	1.52 (1.01)	1.19 (**0.06**)	0.33 (0.00)	0.34 (0.00)	0.002	(3.087)	(0.165)
DCAT-5-Thi	0.60 (**0.05**)	1.48 (0.99)	1.12 (**0.06**)	0.36 (0.01)	0.33 (0.00)	0.002	(3.130)	(0.108)

[a] Numbers in bold font indicate the states presumably relevant for TADF at the T_1 structure.

structures that are incapable of forming intramolecular hydrogen bonds between the CT acceptor/donor units (TPAAP, [0]DCAT, [0]DCAT-1) always yield the highest excitation energies compared to any of the other derivatives of the same subgroup. Adding one cyano group decreases the excitation energy by roughly 0.5 eV in all cases (CAT-1, [1]DCAT, [1]DCAT-1), whereas the addition of the second cyano group has slightly less impact. This is in line with the expectation that cyano groups increase the CT-acceptor strength, thus lowering the energy required for the charge transfer to occur. Secondly, all non-phenyl linkers further lower the excitation energies since the electron-rich heterocycles allow for overall stronger CT-donor units compared to the unmodified TPA donor unit. Here, pyrrole shows the strongest red-shift over furanyl and thiophenyl, which is in agreement with their relative reactivity in electrophilic substitution and thus reflects their succession of donating ability.[15] Overall, our findings suggest a systematic tunability of excitation properties through the choice of linker and substitution pattern in the acceptor.

Focusing on ΔE_{ST} (Fig. 4c), it can be noted that at the S_1 geometry (hatched circles), all of the shown structures feature relatively low gap energies, whereas the behaviour is somewhat different for the TPA-like modifications of the base DCAT structure at the T_1 geometries (hollow diamonds). However, all structures based on DCA-1 indeed show almost the same behaviour at either S_1 or T_1 structure. Note that structures like [0]DCAT-1, which are unable to form hydrogen bonds between CT donor and acceptor units are still found generally suitable with a gap energy below 0.1 eV at both S_1 and T_1 structures.

When comparing the SOCMEs of DCAT molecules with CAT-1, it can be noted that most structures show S_1/T_1 transition (left bar of each pair) of the same order of magnitude (0.1 to 1.0 cm^{-1}; note the logarithmic scale) as the CAT-1 reference. While the pyrrole and furanyl linker versions generally have weaker S_1/T_2 transitions (right bar of each pair), the thiophenyl variants show SOCMEs in the order of 1.0 to 10.0 cm^{-1}. This latter increase is a cause of the heavy atom effect of the sulfur

heteroatom[4] and similar behaviour was found for other sulfur containing molecules in Table S1 of the ESI.†

Next, we investigated the internal reorganization energy λ_{int} for the reverse intersystem crossing (rISC) of each structure as the energy difference between the S_1 state's total energy at the respective T_1 and S_1 optimized structures. Fig. 5(a) and (b) show a double logarithmic plot of λ_{int} *versus* the overall structural change between the singlet and triplet optimized structures in terms of the RMSD value and change in mean hydrogen bond length, respectively.

First of all, it is found that there is a strict correlation between RMSD and reorganization energies, with a large portion of the investigated structures featuring small reorganization energies below 0.1 kcal mol^{-1} and RMSD values below 0.1. Further analyzing the change in the mean hydrogen bond lengths between the S_1 and T_1 structures (*cf.* Fig. 5b) also shows that higher length changes also generally coincide with higher reorganization energies. However, judging by the number of possible hydrogen bonds alone (highlighted by the type of marker) these bonds may not necessarily be the only factor that lead to low reorganization energies in both (a) and (b), as there exist structures with both one as well as zero possible hydrogen bonds that show very low reorganization energies. Considering a series of zero, singly and doubly hydrogen-bonded variants of the same acceptor unit (some examples highlighted by connecting lines in Fig. 5), we typically observe that the step-wise addition of bonds either has only little impact or is strongly stabilizing. The specific behavior is strongly dependent on the acceptor unit though, as for example, the energies in the series for DCAT does not change at all, while DCAT-1 gets stabilized by three orders of magnitude when going from the singly hydrogen-bonded [1]DCAT-1 to the doubly bonded counterpart.

Finally, we investigated the rotation barrier of the π-linker plane between the donor and acceptor units for a sample of molecules (*cf.* Fig. 5c). Here, the linker unit was rotated around its connection axis (see ESI Fig. S2† for a detailed explanation), while the rest of the molecule was frozen at the relaxed ground
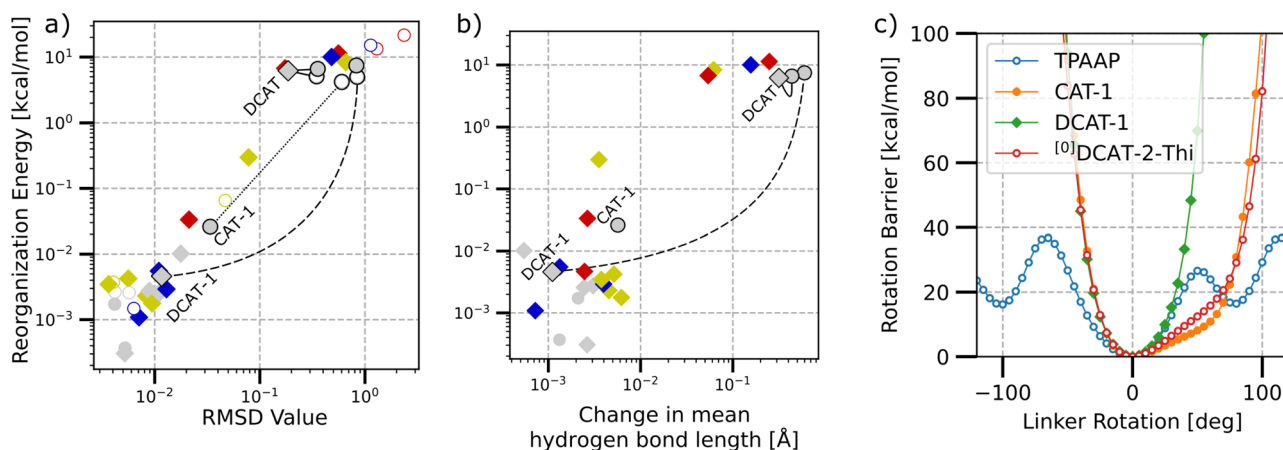

Fig. 5 Double logarithmic plots of internal reorganization energy between the S_1 and T_1 optimized structures and respective structural change in terms of RMSD values (a), change in mean hydrogen bond lengths (b) and primary rotation barrier valley around relaxed structures of selected molecules (c). Diamonds, circles and hollow circles represent structures with two, one and zero hydrogen bonds, respectively. (a and b) Color code applies to different linker types. Annotated and connected data highlights series of two, one and zero bonds.

state geometry. It is found that the phenyl ring in TPAAP may practically rotate freely above 40 kcal mol^{-1} (*i.e.* 1.73 eV, which is similar to the upper bound of NIR to give a perspective). For all other structures, there is a steep gauche-interaction barrier to both directions, as the linker plane eventually would become co-planar and gets repelled by either CN-groups or H-groups of the acceptor and donor units. Surprisingly, CAT-1 and [0]DCAT-2-Thi show almost the same energy profile, despite their rather different designs. While the acceptor in CAT-1 relies on the one CN-group for providing a steric barrier, the acceptor in [0]DCAT-2-Thi architecture features steric barriers through hydrogen atoms to both sides of the linker plane, seemingly leading to a similar trapping situation, despite also the different linker planes themselves. Finally, DCAT-1 features a CN-group on either rotation side, such that the barrier to the right is reached much earlier.

Conclusion

In this study, we investigated the expandability and generality of designing NIR-TADF molecules with one or more intramolecular hydrogen bonds to minimize their rISC-related internal reorganization energy. We conclude that the use of such hydrogen bonds indeed seems to be a useful design strategy for the challenge of designing more rigid NIR-TADF structures, since most bonded structures indeed show an increased rigidity over their non- or singly-bonded counterparts. There is an indication of expandability from one to two bonds, as several of the proposed doubly hydrogen-bonded 4,5-dicyanoanthracene-10-triphenylamine (DCAT) designs reached lower internal reorganization energies than the singly-bonded NIR-TADF molecule CAT-1,[2] that was used as reference for its already exceptional performance.

Nonetheless, the design strategy does unfortunately not hold as a universal design rule, as we identified also structures that did not experience any stabilization through the introduction of one or more intramolecular hydrogen bonds. Therefore, the amount of stabilization is also strongly dependent on the acceptor unit's general design, revealing that the lowering of λ_{int} is correlated but not caused solely by the introduction of hydrogen bonds. Further, studying the rotation barrier of the linker unit's plane between DCA and TPA, we find that the broader DCA acceptor unit and the second CN-group seems to enable even better interlocking of donor and acceptor units. This trapping of the linker also remains effective when substituting for smaller five-membered heterocycles like thiophene, opening the possibility of achieving higher spin–orbit-coupling and transition dipoles through the use of heavy-atom modified TPA donors in exchange for only little rigidity.

Going forward, a more general combined study on both different types and amounts of intramolecular dative bonds (including *e.g.* hydrogen- and halogen-σ-bonds) and their resulting rotational barriers in twisted donor–π–acceptor TADF molecules is desirable, as it might allow to gain a clearer understanding of the relative importances of steric hindrance and intramolecular bonding. Further, the choice of linker size

should be systematically investigated too, as smaller linkers (that are, however, more difficult to trap) in principle allow for shorter effective ranges between the donor and acceptor units which has the potential to improve both the brightness of the S_1 state, as well as the spin–orbit-coupling between the T_1 and S_1 states.

Conflicts of interest

There are no conflicts to declare.

Acknowledgements

Notes and references

1 H. Uoyama, K. Goushi, K. Shizu, H. Nomura and C. Adachi, *Nature*, 2012, **492**, 234–238.

2 D. G. Congrave, B. H. Drummond, P. J. Conaghan, H. Francis, S. T. E. Jones, C. P. Grey, N. C. Greenham, D. Credgington and H. Bronstein, *J. Am. Chem. Soc.*, 2019, **141**, 18390–18394.

3 Y. Luo, S. Li, Y. Zhao, C. Li, Z. Pang, Y. Huang, M. Yang, L. Zhou, X. Zheng, X. Pu and Z. Lu, *Adv. Mater.*, 2020, **32**, 2001248.

4 M. Mońka, I. E. Serdiuk, K. Kozakiewicz, E. Hoffman, J. Szumilas, A. Kubicki, S. Y. Park and P. Bojarski, *J. Mater. Chem. C*, 2022, **10**, 7925–7934.

5 Y. Xiao, H. Wang, Z. Xie, M. Shen, R. Huang, Y. Miao, G. Liu, T. Yu and W. Huang, *Chem. Sci.*, 2022, **13**, 8906–8923.

6 C. Leng, S. You, Y. Si, H.-M. Qin, J. Liu, W.-Q. Huang and K. Li, *J. Phys. Chem. A*, 2021, **125**, 2905–2912.

7 J. Xue, Q. Liang, R. Wang, J. Hou, W. Li, Q. Peng, Z. Shuai and J. Qiao, *Adv. Mater.*, 2019, **31**, 1808242.

8 R. L. Martin, *J. Chem. Phys.*, 2003, **118**, 4775–4777.

9 T.-T. Bui, F. Goubard, M. Ibrahim-Ouali, D. Gigmes and F. Dumur, *Beilstein J. Org. Chem.*, 2018, **14**, 282–308.

10 X. Liang, Z.-L. Tu and Y.-X. Zheng, *Chem.–Eur. J.*, 2019, **25**, 5623–5642.

11 E. D. Glendening, C. R. Landis and F. Weinhold, *Wiley Interdiscip. Rev.: Comput. Mol. Sci.*, 2012, **2**, 1–42.

12 A. Badr Eldin, *Wide Spectra of Quality Control*, IntechOpen, Rijeka, 2011, ch. 13, pp. 237–248.

13 S. Li, X. Jin, Z. Yu, X. Xiao, H. Geng, Q. Liao, Y. Liao, Y. Wu, W. Hu and H. Fu, *J. Mater. Chem. C*, 2021, **9**, 7400–7406.

14 M. Kasha, *Discuss. Faraday Soc.*, 1950, 14–19.

15 L. I. Belen'kii, I. A. Suslov and N. Chuvylkin, *Chem. Heterocycl. Compd.*, 2003, **39**, 36–48.